metals

MDPI

Article

Extracting Al_2O_3 and TiO_2 from Red Mud Smelting Separation Slag by Alkali and Acid Leaching Methods

Siwei Li, Zhengqi Guo *, Jian Pan, Deqing Zhu, Tao Dong and Shenghu Lu

School of Minerals Processing and Bioengineering, Central South University, Changsha 410083, China
* Correspondence: guozqcsu@csu.edu.cn; Tel.: +86-73188836942 or +86-185-7313-1417

Abstract: Recovery of valuable metals from red mud smelting separation slag is important for environmental protection and saving of natural resources. In this paper, we propose a recycling process of red mud smelting separation slag by mineral phase reconstruction conducted under an air atmosphere. In this process, NaOH and $Ca(OH)_2$ roasting of Al_2O_3 and $NaAlSiO_4$ was performed, and Al_2O_3 and SiO_2 were converted into alkaline-soluble $NaAlO_2$ and Ca_2SiO_4, respectively. In the consequent steps, more than 80% of Al_2O_3 was selectively dissolved into a leaching solution using a NaOH solution under 95 °C, and the obtained $NaAlO_2$ solution can be used as a source for extracting alumina. Then, a 20 wt.% HCl solution was used to remove SiO_2 from the residue, obtaining a SiO_2-containing solution and a concentrated residue of undissolved TiO_2 and CaO. Finally, this mineral phase reconstruction process can enable a higher metal leaching rate, and this study provides a novel, clean, and sustainable method for recycling valuable metals from red mud smelting separation slag.

Keywords: red mud; smelting separation slag; mineral phase reconstruction; separational extraction; cleaner process

check for updates

Citation: Li, S.; Guo, Z.; Pan, J.; Zhu, D.; Dong, T.; Lu, S. Extracting Al_2O_3 and TiO_2 from Red Mud Smelting Separation Slag by Alkali and Acid Leaching Methods. *Metals* **2023**, *13*, 552. https://doi.org/10.3390/met13030552

Academic Editor: Jean François Blais

Received: 3 February 2023
Revised: 27 February 2023
Accepted: 1 March 2023
Published: 9 March 2023

Copyright: © 2023 by the authors. Licensee MDPI, Basel, Switzerland. This article is an open access article distributed under the terms and conditions of the Creative Commons Attribution (CC BY) license (https://creativecommons.org/licenses/by/4.0/).

1. Introduction

Bauxite residue (Red mud (RM)) is generated as hazardous waste from the Bayer process to extract alumina. It is estimated that 0.8–1.5 tons of RM are generated per ton of produced alumina [1–3]. Table 1 shows the annual generation of RM in some countries for 2022 year [4]. Statistical data indicate that the RM output in China was 105 million tons in 2018, while it is estimated that 480–870 million tons of RM remain untreated. In addition, the RM contains several valuable metals, such as iron, aluminum, and titanium, representing a valuable secondary resource for recycling and utilization [5–8]. Therefore, considering the environmental protection requirement and the depletion of high-quality metal resources, it is highly desirable to minimize the amount of RM hazardous waste and reuse it for extracting important metals.

Table 1. Annual production of RM in different countries for 2022 year.

Country	Amount (Millon Tonnes)
Africa & Asia (ex China)	11.03–20.69
North America	1.93–3.62
South Americal	9.31–17.45
Europe (inc Russia)	6.58–12.33
Oceania	16.10–30.17
China	63.81–119.64

Landfilling or stockpiling is the primary disposal method of RM, but it pollutes the environment and leads to resource wasting. Therefore, significant research was devoted to finding cost-efficient and environmentally sustainable processes that can help properly utilize and dispose of the RM. These methods can be classified into four types, namely

construction materials, absorbents, catalysts, and recovering valuable elements [8]. The first three methods use a small amount of RM, so the recovery of valuable elements has attracted widespread attention.

The separation of iron and aluminum is a crucial step to realize the comprehensive utilization of RM without secondary tailings. Iron in RM mainly exists in the form of hematite and goethite. Aluminum is dominantly present as boehmite, and the output form was mixed inlaid with goethite and hematite, showing a gradual transitional intergrowth relationship [9,10]. Overall, the close association of iron- and aluminum-bearing minerals results in the problematic separation of iron from aluminum by traditional beneficiation processes. According to the mineral processing and separation theory, a high-temperature treatment can change iron properties and broaden the difference window in physical and chemical properties compared to aluminum-bearing minerals, thereby enabling the separation of iron and aluminum. Therefore, many researchers focused on the pyrometallurgical process to treat RM, where iron is recovered in the form of metallic iron and pig iron [11–13]. Unfortunately, in these pyrometallurgical processes, Al-bearing minerals from RM easily form corundum, mullite, and nepheline, which are difficult to recover by direct alkaline leaching, yielding a lower Al_2O_3 recovery rate [14–16]. Bacia et al. [17] studied the effect of leaching conditions on the extraction of aluminum compounds using NaOH solutions at atmospheric pressure. The results show that the optimal conditions were leaching at 80 °C for 4 h and NaOH concentration of 10 M (400 g/L) and the Al recovery rate was only 67.3%. The experiments of red mud autoclave leaching by 40–60% NaOH solution in the temperature range of 170–210 °C with lime milk addition has shown the recovery of 87.5% for Al_3 [18]. Considering the growth in China's aluminum consumption and the depletion of high-quality bauxite, the dependence on external Al resources has reached 60%. Therefore, the comprehensive utilization of secondary Al-bearing resources or Al-enriched slag can relieve the pressure of insufficient resources, which is significant for promoting the sustainable development of China's aluminum industry.

In our previous work, Al-enriched slag from RM was successfully prepared through pre-reducing-smelting separation, and it can be used as a feed for extracting Al_2O_3 [19]. In this work, we aim to find a novel process to treat Al-enriched slag efficiently. Meanwhile, the mechanism of corundum and nepheline reconstruction with NaOH and $Ca(OH)_2$ was investigated, and the effects of alkaline leaching parameters on the recovery of Al_2O_3 and SiO_2 were optimized. Based on that, a modified alkaline leaching process was proposed to extract Al_2O_3 from the smelting separation slag of RM.

2. Materials and Methods

2.1. Materials

2.1.1. Smelting Separation Slag

Based on our previous study, pre-reducing-smelting separation was performed to recover iron from RM (reducing temperature at 1200 °C, smelting separation at 1600 °C with 0.7 basicity), and we simultaneously obtained smelting separation slag (SSS) [19]. The chemical composition of SSS is shown in Table 2. The SSS contains 47.60% Al_2O_3, 9.53% SiO_2, and 10.35% TiO_2. The X-ray diffraction (XRD) pattern of the slag is shown in Figure 1. The main mineral phase is corundum (Al_2O_3). In addition, there is a small amount of nepheline ($NaAlSiO_4$) and perovskite ($CaTiO_3$) phases. The occurrence and the mineral phase of Al_2O_3 and SiO_2 in SSS are listed in Table 3. Alumina exists primarily as an insoluble aluminum phase, while silica occurs mainly in the form of silicate.

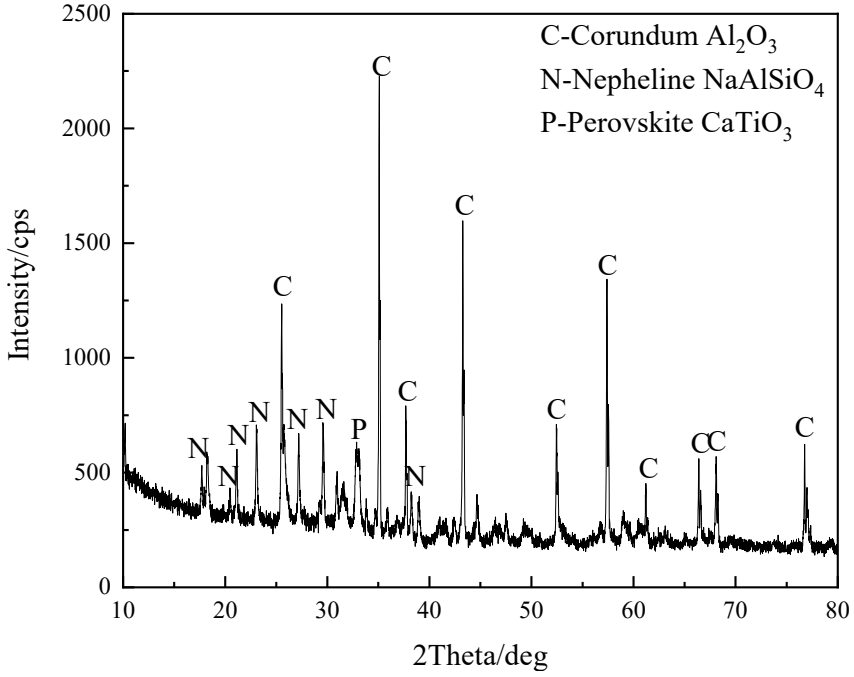


Figure 1. XRD pattern of the SSS.

Table 2. Main chemical composition of SSS (%).

Fe	Al_2O_3	SiO_2	CaO	MgO	K_2O	Na_2O	TiO_2	P	S
2.65	47.60	9.53	6.38	0.56	0.13	4.08	10.35	0.079	0.15

Table 3. Occurrence of alumina and silica in the SSS (%).

	Alkaline-Soluble	Insoluble	Total
Al_2O_3 content	3.17	44.43	47.60
Fraction	6.67	93.33	100
	Free SiO_2	Silicate	Total
SiO_2 content	0.18	9.35	9.53
Fraction	1.89	98.11	100

The electron probe microanalysis (EPMA) of SSS is presented in Figure 2. Aluminum is combined with oxygen, forming corundum. The silicon content is low, exhibiting scattered and non-uniform distribution. Titanium and calcium are combined, forming the perovskite phase. There is a clear boundary between the corundum and perovskite phases, which is conducive to the subsequent mineral phase reconstruction.

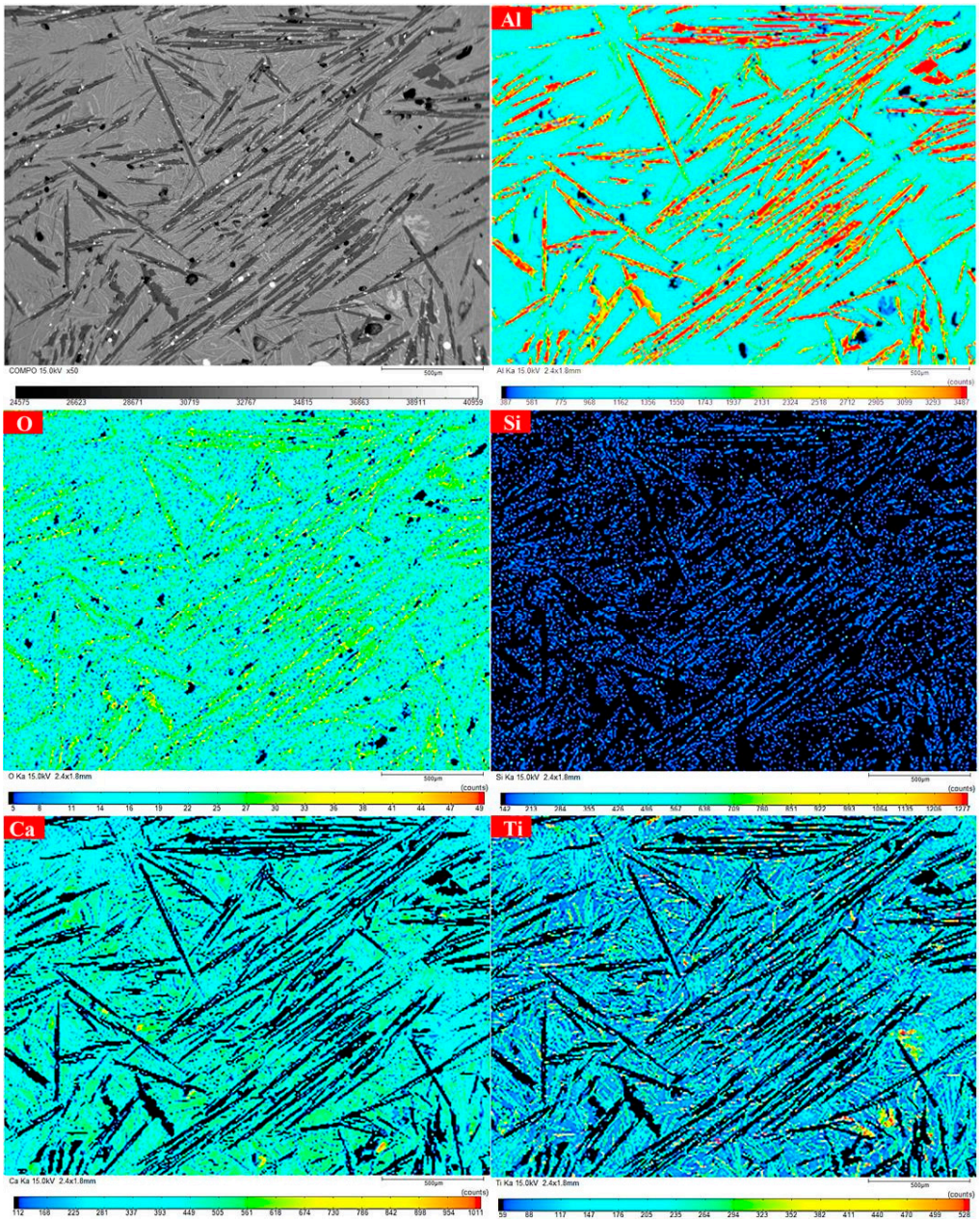


Figure 2. EPMA of the SSS.

2.1.2. Additives

Analytical grade NaOH and $Ca(OH)_2$ were used as additives in this paper for reconstructing the Al-bearing mineral phase in the SSS. The fineness of these additives is below 200 mesh.

2.2. Methods

The pre-reduction-smelting separation procedure used for the SSS preparation was described in detail in the reference [19]. The experimental flowsheet is shown in Figure 3. The extraction process of aluminum from the SSS includes two steps: (1) roasting the slag with NaOH and $Ca(OH)_2$ additives for the mineral phase reconstruction; (2) alkaline leaching of the modified slag for Al_2O_3 extraction.

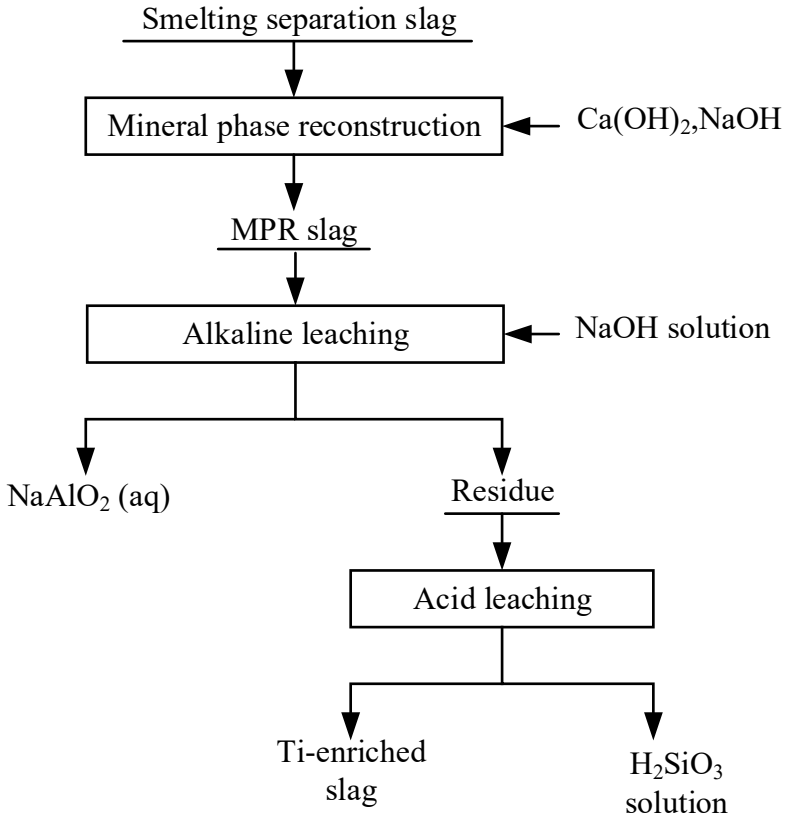


Figure 3. Experimental flowsheet of the proposed SSS treatment process.

Mineral phase reconstruction: The SSS (75% below 200 mesh) and additives were mixed thoroughly, and then the mixtures were molded in pellets using a cylinder with a diameter of 10 mm and a height of 10 mm. These pellets were dried at 105 °C for 4 h, and then the dry pellets were prepared for modification. Approximately 30 g of dry pellets were loaded into a corundum crucible and roasted in a pipe furnace at a set temperature (1150–1300 °C) for a specific time (15–60 min) and then cooled down to ambient temperature.

Alkaline leaching: About 20 g of the mineral phase reconstruction slag (MPRS) was leached in an alkaline solution with a specific concentration at a set temperature (65–95 °C) for a specific time (60–150 min) at a fixed stirring speed of 400 rpm. After the pulp filtration, the leaching residue was washed with deionized water. The extraction rate of Al_2O_3 and SiO_2 was calculated as follows:

$$\eta = \left(100 - \frac{y_1 \times w_1}{w_0}\right) \times 100\% \quad (1)$$

where η is the extraction rate of Al_2O_3 (or SiO_2); y_1 is the yield of the alkaline leaching residue; w_0 and w_1 are the contents of Al_2O_3 (or SiO_2) in the MPRS and the alkaline leaching residue, respectively.

Acid leaching tests: About 20 g of the alkaline leaching slag was then leached in an acid solution with a specific concentration. This mixture was stirred at a rate of 400 rpm for a time in the range of 15–60 min, and at a temperature in the range of 30–90 °C. After filtration of the leaching pulp, the acid leaching residue was washed with deionized water, dried, and then weighed. This dried product was the enrich TiO_2 concentrate, which was used for further analyses.

2.3. Characterization

X-ray fluorescence spectroscopy (XRF, PANalytical Axios; RIGAKU ZSX Priums, PANalytical B.V., Almelo, The Netherlands) was used to measure the chemical composition of all the slags. The mineral composition and elemental distribution characteristics of Al_2O_3 and SiO_2 in these slags were measured by chemical analysis based on the handbook of the chemical phase analysis of slag [20,21]. The particle size of the leaching residue was measured by a laser particle analyzer (Mastersizer, 2000, Malvern, Malvern city, United Kingdom). The phase compositions of the various slags were determined using an X-ray diffractometer (XRD, RIGAKU, D/Max-2500, Bruker corporation, Madison, WI, USA). The elemental distribution of the SSS was examined by electron probe microanalysis (EPMA) (JXA-8230, Shimadzu, Kyoto, Japan). The alkaline solubility characteristics of MPRS were measured by chemical analysis based on the reference [22]. The structure of Al and Si of SSS and MPRS was determined by Fourier transform infrared spectrometry (FTIR) (Perkin-Elmer Spectrum GX, Thermo, Waltham, MA, USA) and Raman spectrometry (Fischer DXR, Thermo, Waltham, MA, USA). The changes in the coordination of Al and Si of SSS and MPRS were investigated by NMR (Avance NEO 600, Bruker, Karlsruhe, Germany).

3. Results and Discussion

3.1. Mineral Phase Reconstruction Procedure

In the SSS, aluminum exists mainly as corundum (Al_2O_3) and nepheline ($NaAlSiO_4$) phases. Hence, the detailed reactions between Al-bearing minerals with Na/Ca additives are demonstrated in this study. Equations (2)–(9) show the possible reactions during the reconstruction process of Al_2O_3 and $NaAlSiO_4$, and FactSage 8.0 software (Thermfact/CRCT, Montreal, QC, Canada; GTT-Technologies, Herzogenrath, Germany) was used to calculate the changes in the Gibbs free energy of the reactions, and the results are shown in Figure 4. According to the thermodynamic calculations, Al_2O_3 reacts preferentially with Na_2O or NaOH, forming than $NaAlSiO_4$. The Gibbs free energy ($\Delta_rG_m{}^\theta$) of Equations (2)–(5) is negative, indicating that the reaction can occur during the range of modification temperatures. Compared with Al_2O_3, the $NaAlSiO_4$ reacts preferentially with CaO or $Ca(OH)_2$, and the $\Delta_rG_m{}^\theta$ of Equations (6) and (7) are negative. The $\Delta_rG_m{}^\theta$ values of Equations (8) and (9) decrease as the temperature increases, indicating that the reaction is more favorable at high temperatures. Considering the separation of Al and Si in the subsequent alkaline leaching process, Na and Ca bearing additives are used together.

$$Al_2O_3 + Na_2O = 2NaAlO_2 \quad (2)$$

$$NaAlSiO_4 + Na_2O = NaAlO_2 + Na_2SiO_3 \quad (3)$$

$$Al_2O_3 + 2NaOH = 2NaAlO_2 + H_2O \quad (4)$$

$$NaAlSiO_4 + 2NaOH = NaAlO_2 + Na_2SiO_3 + H_2O \quad (5)$$

$$Al_2O_3 + CaO = CaO{\cdot}Al_2O_3 \quad (6)$$

$$NaAlSiO_4 + 2CaO = NaAlO_2 + Ca_2SiO_4 \quad (7)$$

$$Al_2O_3 + Ca(OH)_2 = CaO{\cdot}Al_2O_3 + H_2O \quad (8)$$

$$NaAlSiO_4 + 2Ca(OH)_2 = NaAlO_2 + Ca_2SiO_4 + 2H_2O \quad (9)$$

As aluminum mainly exists as corundum (Al_2O_3) and nepheline ($NaAlSiO_4$) phases, it is difficult to extract Al_2O_3 from the SSS by direct leaching. In this paper, Na and Ca-bearing additives were added to the slag to reconstruct the mineral phases of Al-bearing and Si-bearing minerals and selectively extract Al_2O_3. The roasted slags prepared at different conditions were leached at 95 °C for 2 h in an alkaline solution with a concentration of 2 mol/L and with a liquid-to-solid ratio of 10 mL/g.

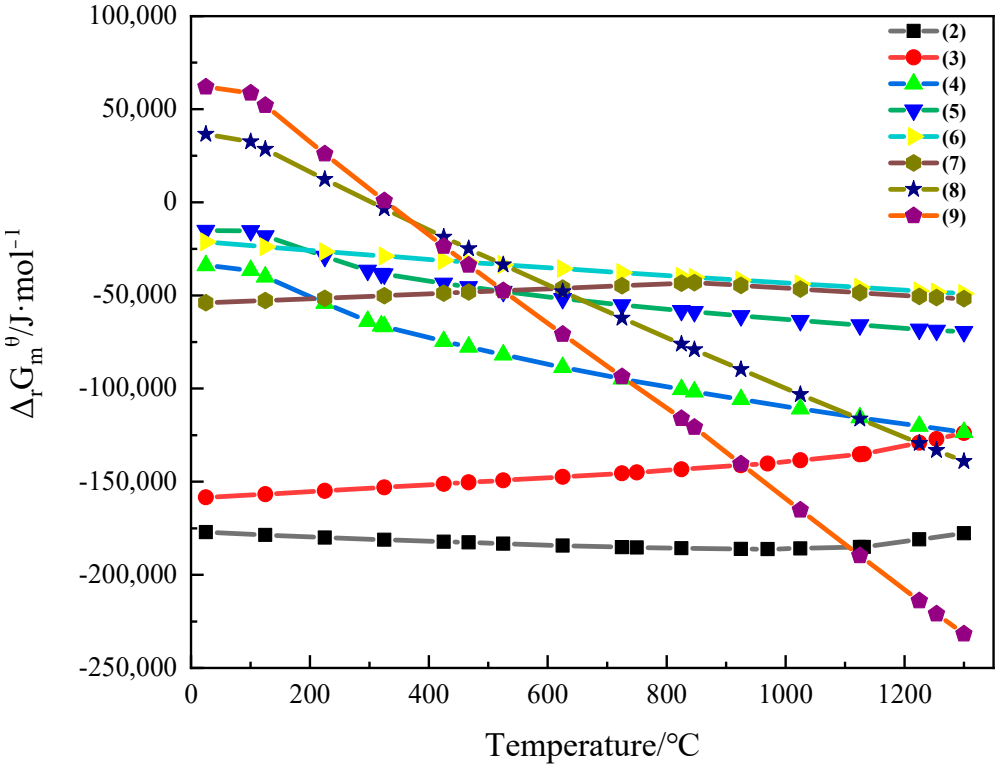


Figure 4. Change of the standard Gibbs free energies of possible reactions (2)–(9) in the modified process.

The effect of roasting temperature on the leaching ratio of Al_2O_3 and SiO_2 is shown in Figure 5a. As shown in Figure 5a, the yield of the alkaline leaching residue decreases from 63.10 to 59.12% with a temperature increase from 1150 to 1300 °C. Meanwhile, the leaching rate of Al_2O_3 and SiO_2 increases from 59.78 and 8.84% to 64.83 and 15.49%, respectively. Figure 5b shows that the content of Al_2O_3 decreases with elevating the temperature from 1150 to 1250 °C, indicating that most Al-bearing minerals achieve the mineral phase reconstruction, increasing the Al_2O_3 leaching rate. As the temperature increases from 1250 to 1300 °C, the content of SiO_2 increases due to the mullite decomposition. Meanwhile, the increase in the SiO_2 leaching rate results in poor Al extraction selectivity by alkaline leaching. Therefore, the recommended optimal roasting temperature is 1200 °C.

Figure 5c shows the effect of roasting duration on the Al_2O_3 extraction. The yield of alkaline leaching residue decreases from 63.65 to 55.81%, prolonging the roasting time from 15 to 60 min. Meanwhile, the leaching rate of Al_2O_3 increases from 53.96 to 70.66%, as shown in Figure 5c. The content of Al_2O_3 decreases with prolonging the duration from 15 to 60 min, meaning that a long roasting time is beneficial to improve the transformation of corundum (Al_2O_3) and nepheline ($NaAlSiO_4$) to sodium aluminate ($NaAlO_2$), as shown in Figure 5d. Overall, the suggested optimal roasting time is 60 min.

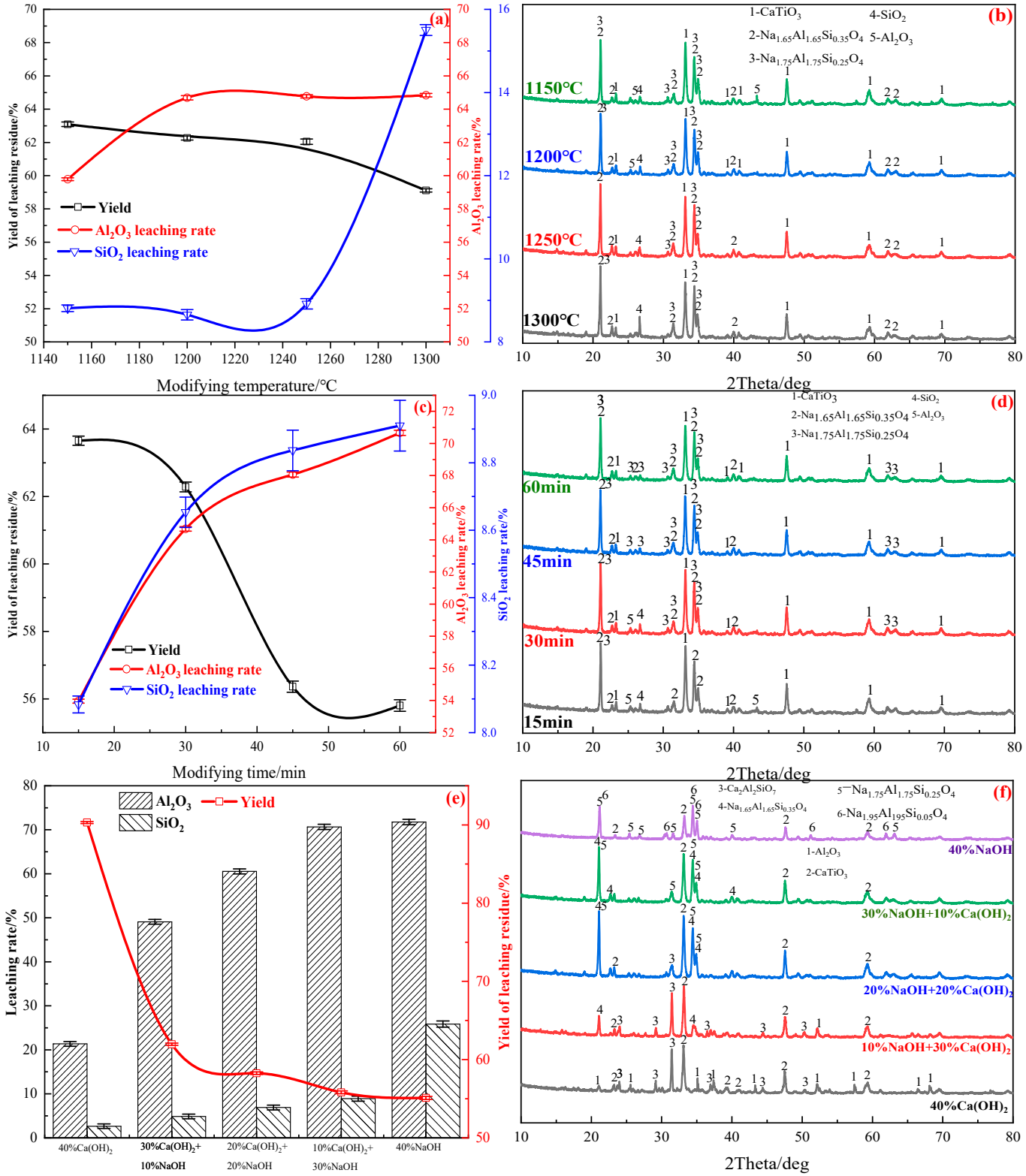


Figure 5. Effect of roasting parameters on the extraction of Al_2O_3 and mineral compositions ((**a**,**c**,**e**): extraction of Al_2O_3, (**b**,**d**,**f**): mineral composition). ((**a**): 30% NaOH + 10%Ca(OH)$_2$, modifying duration of 30 min; (**c**): 30% NaOH + 10% Ca(OH)$_2$, modifying at 1200 °C; (**e**): modifying at 1200 °C for 60 min).

The effect of additives on the Al_2O_3 extraction is shown in Figure 5e. The yield of the alkaline leaching residue decreases from 90.30 to 55.10% with an increase of the

NaOH dosage from 0 to 40%. Meanwhile, the leaching rate of Al_2O_3 and SiO_2 increases from 21.34 and 2.65% to 71.75 and 25.8%, respectively. Figure 5f shows that the mineral phases of the roasted slag obtained at a 40% $Ca(OH)_2$ dosage are $Ca_2Al_2SiO_7$, Al_2O_3, and $CaTiO_3$. Increasing the NaOH dosage to 10%, the diffraction peak intensity of Al_2O_3 and $Ca_2Al_2SiO_7$ decreases, while the diffraction peak of $Na_{1.65}Si_{1.65}Al_{0.35}O_4$ appears. By further increasing the NaOH dosage to 20%, the diffraction peak intensity of $Ca_2Al_2SiO_7$ keeps decreasing, while the diffraction peak of Al_2O_3 disappears. At 30% NaOH and 10%$Ca(OH)_2$, the mineral phases of the modified slag are $Na_{1.65}Si_{1.65}Al_{0.35}O_4$, $Na_{1.75}Si_{1.75}Al_{0.25}O_4$, and $CaTiO_3$. The diffraction peak of $Na_{1.65}Si_{1.65}Al_{0.35}O_4$ is transformed to $Na_{1.95}Si_{1.95}Al_{0.05}O_4$ with an additive content of 40% NaOH. Increasing the NaOH dosage is beneficial to promoting the reconstruction of Al-bearing minerals. However, when only NaOH is added, the leaching rate of SiO_2 is 25.80%, indicating that solely adding NaOH disrupts the selective extraction of aluminum. Therefore, the recommended optimal additive contents are 30% NaOH and 10% $Ca(OH)_2$.

The MPRS was obtained by roasting the SSS at 1200 °C for 60 min with 30% NaOH and 10% $Ca(OH)_2$. The mineral phases of the MPRS determined are shown in Figure 5f. The main mineral phases are $Na_{1.65}Al_{1.65}Si_{0.35}O_4$, $Na_{1.75}Al_{1.75}Si_{0.25}O_4$, and $CaTiO_3$. The mineral phases of Al_2O_3 and SiO_2 in these phases in the MPRS are listed in Table 4. Compared with the SSS, the soluble Al_2O_3 increases in the MPRS, and the silicate content changes slightly, indicating that adding Ca^{2+} and Na^+ can promote the transformation of corundum (Al_2O_3) and nepheline ($NaAlSiO_4$) phases to soluble Al_2O_3. The detailed mechanism of the modification process is described as follows:

Table 4. Occurrence of alumina and silica in the MPRS (%).

	Alkaline-Soluble	**Insoluble**	**Total**
Al_2O_3 content	31.53	4.93	36.46
Fraction	86.47	13.53	100
	Free SiO_2	Silicate	Total
SiO_2 content	0.13	7.16	7.29
Fraction	1.83	98.17	100

The functional groups of the SSS and MPRS were examined by FTIR spectroscopy (Figure 6a). The peaks at 3320 and 1668 cm^{-1} belong to the stretching vibration of the O-H band in hydroxyl groups and water absorbed on the surface of SSS, respectively. The absorption peaks at 950 and 422 cm^{-1} are related to the antisymmetric vibration of Si-O and the bending vibration of Si-O-Si, respectively. The vibration peaks at 537 and 653 cm^{-1} originate from the vibration of Ti-O-Al and the stretching vibration peaks of Al-O in the aluminum oxide octahedron [AlO_6]. In the FTIR spectrum of the MPRS, the absorption peak at 968 cm^{-1} belongs to the antisymmetric vibration of Si-O; a small shift exists compared to that of SSS due to the influence of Ca^{2+} and Na^+ from the additives, indicating that the Si-O network is gradually split and depolymerized, forming Si-O-Ca after modifying. The absorption peak at 851 cm^{-1} is related to the symmetric stretching vibration of Al-O-Al, indicating that the amount of Al^{3+} participating in the formation of sodium aluminate is increased, facilitating the dissolution of Al_2O_3 in the leaching process [23–25].

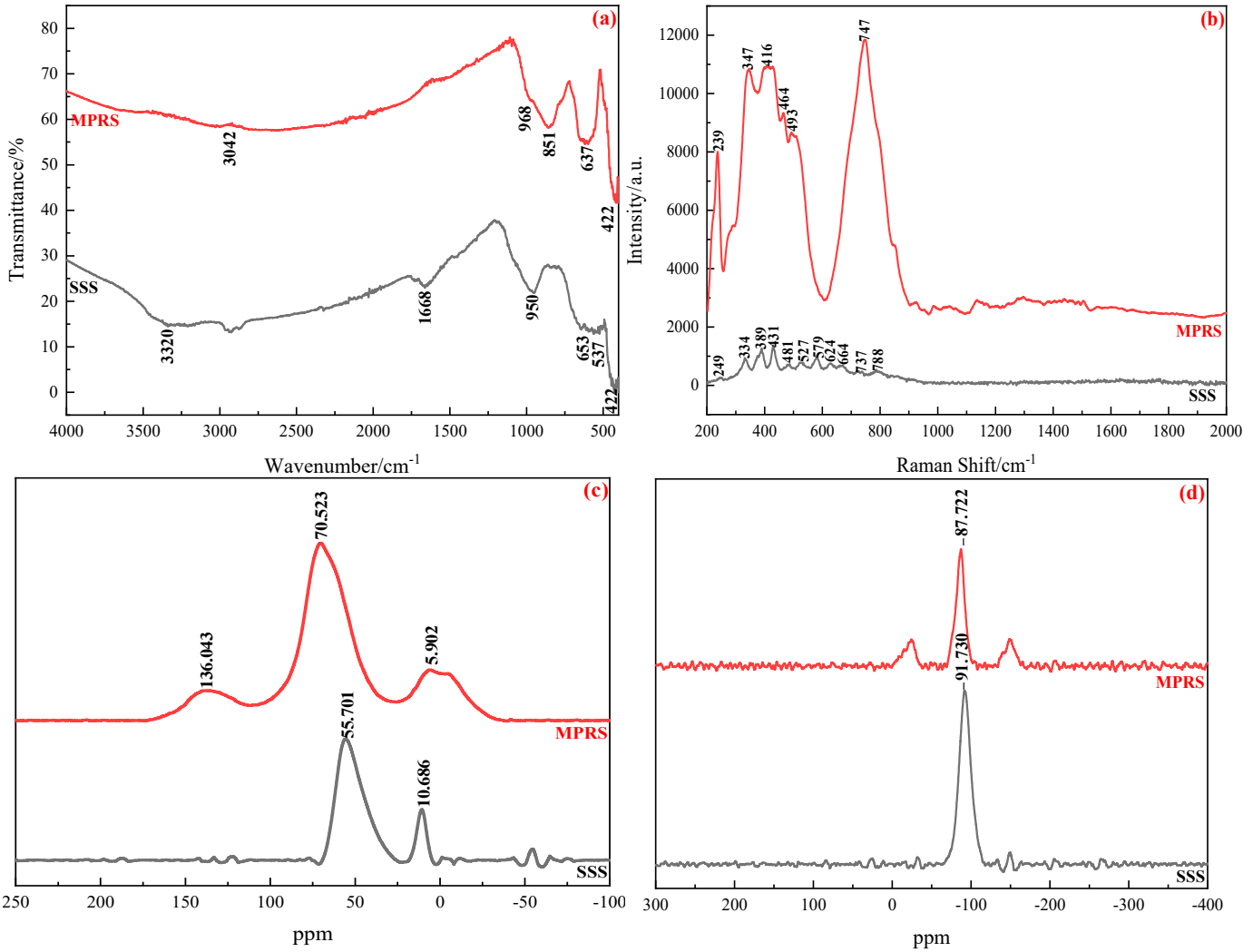


Figure 6. Spectral analysis in the SSS and MPR slags ((**a**): FTIR, (**b**): Raman, (**c**): NMR pattern of ^{27}Al, (**d**): NMR pattern of ^{29}Si).

Raman spectroscopy was applied to get better insight into the functional groups of the two slags, and the results are shown in Figure 6b. The peaks at 334 and 389 cm^{-1} belong to the stretching vibration of Si-O in the SSS. The peaks at 431 and 481 cm^{-1} are related to the Si-O-Si bending vibration, cation participation, and its long-range-ordered framework vibration. The peaks in the range of 524–700 cm^{-1} belong to the antisymmetric stretching vibration of Al-O. Compared with the wavenumber shifts of SSS, the wavenumber shifts of Al-O disappear. The width and intensity of Ti-O, Si-O, and Al-O-Si vibration peaks increase with the addition of Ca^{2+} and Na^{+}, implying that the activities of Al_2O_3 and SiO_2 increase, increasing the leaching rates of Al_2O_3 and SiO_2 [26,27].

Figure 6c,d show the MAS NMR spectra of ^{27}Al and ^{29}Si in the two slags. The chemical shifts of ^{27}Al in the SSS are 55.70 ppm and 10.69 ppm, the former assigns to 4-coordinated (tetrahedral) Al, and the latter belongs to 6-coordinated (octahedral) Al species. The chemical shift of ^{29}Si is −91.73 ppm, which belongs to the Q^3 layer groups. Compared with the SSS, an increase of the 4-coordinated Al content and a corresponding decrease for Al in 6-coordinated appear in the MS, indicating that alumina becomes more active. The chemical shift of ^{29}Si in the MPRS belongs to the Q^2 chain-shaped structure. The different chemical shifts represent the silicon Q^n environments, where n is the number of bridging oxygen atoms linked to other Si atoms for each $Q(SiO_4)$ unit [28,29]. The difference in the Si structure between SSS and MPRS indicates that the polymerization degree of the MPRS

is lower than that of the SSS. Meanwhile, the Ca-O-Si bond is formed. The results agree with the FTIR spectra.

In summary, the addition of Ca^{2+} and Na^{+} has a significant influence on the structural change of the SSS and is conducive to the transformation of corundum and nepheline to sodium aluminate and calcium silicate.

3.2. Alkaline Leaching of the MPR Slag

The effect of leaching temperature is examined in the ranges from 65 to 95 °C at a NaOH concentration of 4 mol/L, a liquid-to-solid ratio of 10 mL/g, and a 75%-particle size less than 200 mesh. The results are shown in Figure 7. It can be seen that prolonging the leaching time positively impacts the Al_2O_3 recovery rate. The Al_2O_3 recovery is 66.50% at a leaching temperature of 65 °C for 120 min. Meanwhile, the recovery of Al_2O_3 is 80.66% at a leaching temperature of 95 °C, indicating that high temperature is conducive to the extraction of Al_2O_3.

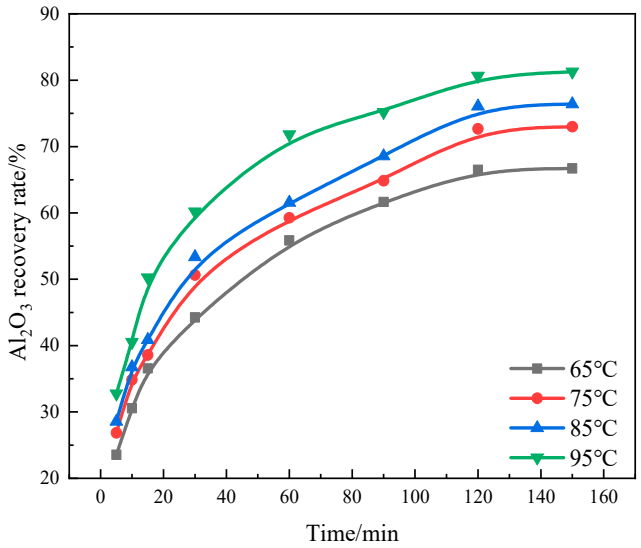


Figure 7. Plots of the leaching rate of Al_2O_3 of the modified slag versus the leaching temperature and time.

According to the experimental data from Figure 7, the plots of $1-(1-x)^{1/3}-t$ and $1-2x/3-(1-x)^{2/3}-t$ are depicted in Figure 8, and the G(a)-t correlation coefficient is shown in Table 5. The plot of $1-2x/3-(1-x)^{2/3}-t$ exhibits an excellent linear relation, indicating that the leaching process is controlled by internal diffusion.

Table 5. The G(a)-t correlation coefficient obtained from the linear fit of the Al_2O_3 leaching rate of the MPRS.

	65 °C		75 °C		85 °C		95 °C	
	R^2	k	R^2	k	R^2	k	R^2	k
$1-(1-x)^{1/3}$	0.9111	0.0015	0.9312	0.0017	0.9362	0.0019	0.8987	0.0020
$1-2x/3-(1-x)^{2/3}$	0.9510	0.0005	0.9657	0.0006	0.9679	0.0007	0.9395	0.0008

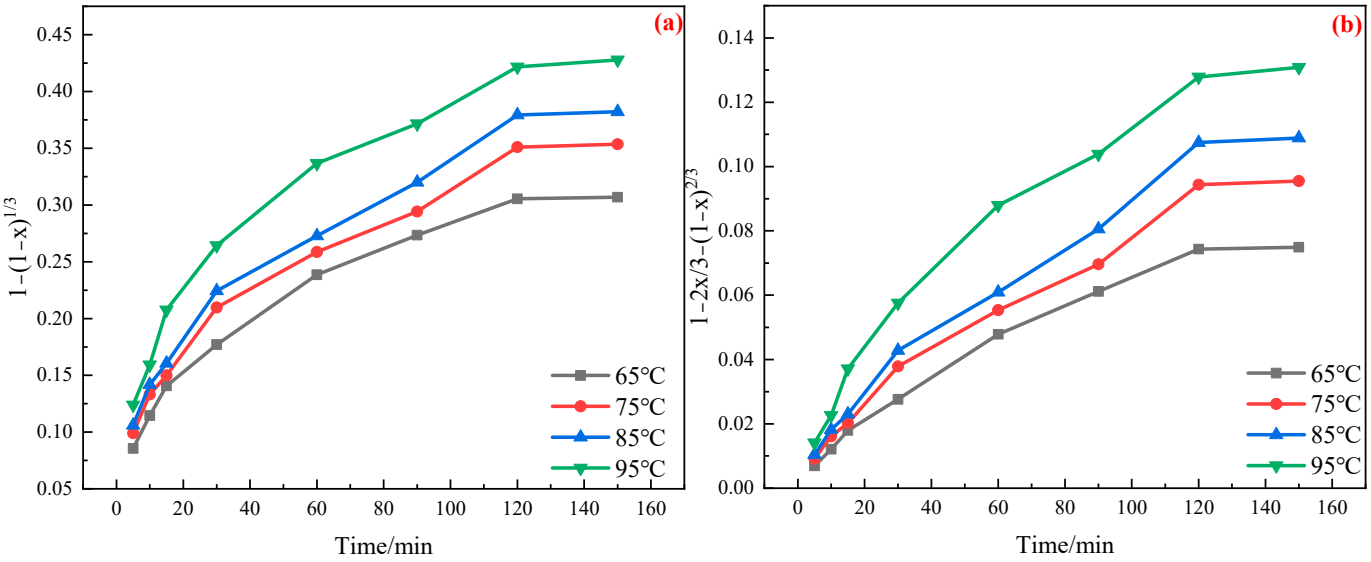


Figure 8. G(a)-t lines of the Al_2O_3 leaching rate of the MPRS under 65–95 °C ((**a**): $1 - (1 - x)^{1/3} - t$, (**b**): $1 - 2x/3 - (1 - x)^{2/3} - t$).

To calculate the apparent activation energy, the plot of lnk-1/T should be a straight line with a slope of -E/R and an intercept of lnk_0. According to the Arrhenius equation and Table 5, the linear fitting between lnk-1/T was calculated and presented in Figure 9. The apparent activation energy of the leaching process is 16.21 kJ/mol, which agrees with the results presented in the reference [30] when the reaction process is controlled by internal diffusion. According to the results in Figure 7, the following kinetic expression can be derived to describe the leaching process: $1 - 2x/3 - (1 - x)^{2/3} = [1.61 \times 10^{-2} \times \exp(-1949.72/T)] \times t$.

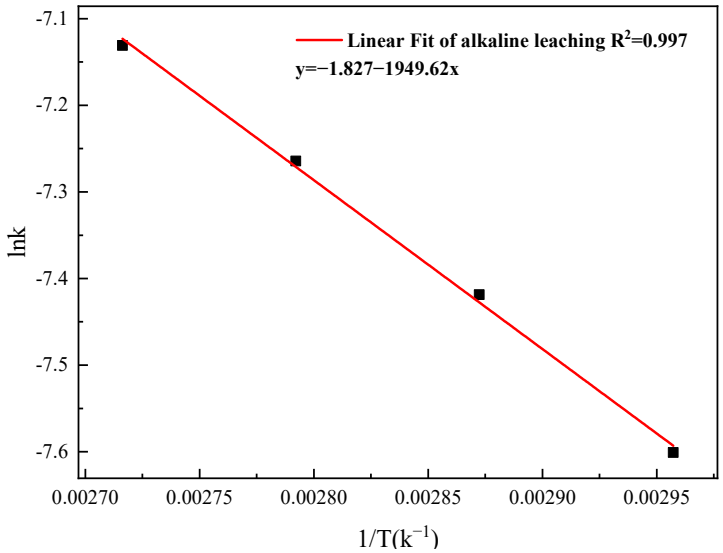


Figure 9. Plots of lnk versus 1/T of the Al_2O_3 leaching rate.

The leaching process was controlled by the internal diffusion of the liquid reactant through the reaction interface. Some parameters were optimized, such as alkaline concentration, leaching temperature, time, liquid-to-solid ratio, and particle size, to improve the Al_2O_3 extraction.

Fixing the liquid-to-solid ratio at 10 mL/g and a 75% particle size less than 200 mesh, the MPR slag was leached at 95 °C for 120 min. The effect of the alkaline concentration on

the recovery of Al_2O_3 is illustrated in Figure 10a. The yield of leaching residue decreases from 59.49 to 47.70% with an increase in the alkaline concentration from 2 to 4 mol/L. Meanwhile, the leaching rates of Al_2O_3 and SiO_2 increase from 70.66 and 8.93% to 80.66 and 10.29%, respectively. The Al_2O_3 content in leaching residue decreases from 17.57 to 14.78%. However, the SiO_2 content increases from 10.90 to 13.71%. Further increasing the alkaline concentration has a slight impact on the indexes. The dissolution rate of sodium aluminosilicate increases with the alkaline concentration. However, increasing the alkaline concentration further has little effect on the dissolution rate of sodium aluminosilicate, although it raises the operation cost. Therefore, the recommended optimal alkaline concentration is 4 mol/L.

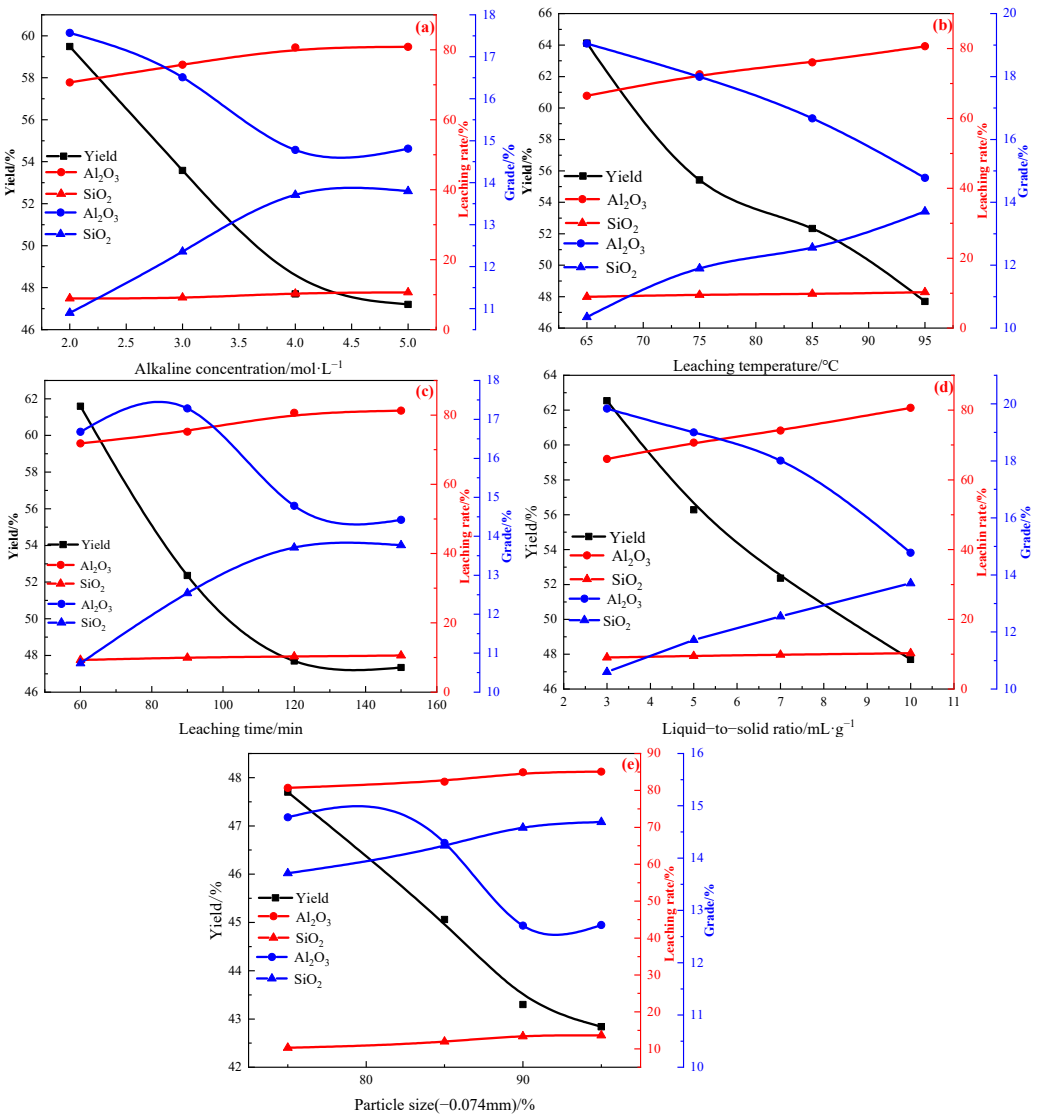


Figure 10. Effects of alkaline leaching parameters on the extraction of Al_2O_3 ((**a**): alkaline concentration, (**b**): leaching temperature, (**c**): leaching time, (**d**): liquid-to-solid ratio, (**e**): particle size).

As shown in Figure 10b, the leaching temperature is 65 °C, and the leaching residue yield is 64.12%. The corresponding leaching rates of Al_2O_3 and SiO_2 are 66.50 and 8.97%, respectively, and the grade of Al_2O_3 and SiO_2 is 19.05 and 10.35%, respectively. By increasing the temperature to 95 °C, the yield decreases to 47.70%. The leaching rates of Al_2O_3 and SiO_2 increase to 80.66 and 10.29%. Meanwhile, the grade of Al_2O_3 and SiO_2 is 14.78 and 13.71%, respectively. The leaching rate of sodium aluminosilicate increases with

the leaching temperature, enhancing the leaching rate of Al_2O_3. Therefore, the proposed optimal leaching temperature is 95 °C.

The effect of leaching time on the recovery of Al_2O_3 is illustrated in Figure 10c. The yield decreases from 61.59 to 47.70% with an increase in the leaching time from 60 to 120 min. The leaching rates of Al_2O_3 and SiO_2 increase from 71.82 and 9.26% to 80.66 and 10.29%, respectively. Prolonging the leaching time to 150 min, these indexes change slightly. Therefore, the proposed optimal leaching time is 120 min.

As shown in Figure 10d, the leaching rate of Al_2O_3 increases rapidly as the liquid-to-solid ratio raises from 3 to 10 mL/g. Moreover, as the liquid-to-solid ratio increases, the content of NaOH increases, and the particles possess a higher contact area to react with NaOH. Therefore, the optimal liquid-to-solid ratio is 10 mL/g.

It can be seen from Figure 10e that the leaching rates of Al_2O_3 and SiO_2 increase from 80.66 and 10.29% to 84.91 and 13.40%, respectively, with the particle size increasing from 75 to 90%, passing through a 200 mesh. According to the dynamic model, the leaching process is controlled by internal diffusion. When the particle size is refined, the diffusion rate increases, and the energy barrier required for the reaction decreases. Therefore, the optimal particle size is set at 90%, passing through a 200 mesh.

The main chemical composition of various leaching residues is presented in Table 6. The content of TiO_2 and CaO of the alkaline leaching residue is 17.97 and 16.81%, respectively, exhibiting high utilization values. However, there is no effective measure to recover calcium and titanium from RM. In addition, it also contains 12.71% Al_2O_3, 14.58% SiO_2, and 14.54% Na_2O, respectively. According to the acid solubility difference between perovskite and gangue, the subsequent acid leaching can further remove Al_2O_3 and SiO_2 to enrich TiO_2. Keeping the liquid-to-solid ratio at 10 mL/g, the leaching is performed at 30 °C for 30 min using 20 wt.% HCl to remove Al_2O_3 and SiO_2, while CaO and TiO_2 remain in the residue. The acid-leaching residue contains 46.53% TiO_2 and 37.21% CaO. The main impurities in TiO_2 were 6.04% Fe, 4.8% Al_2O_3, and 0.81% SiO_2. To compare the mineral phase composition before and after acid leaching, XRD patterns are presented in Figure 11. Before acid leaching, the main mineral phase is perovskite. In addition, there is a small amount of $NaAlSi_3O_8$. However, the diffraction peaks of $NaAlSi_3O_8$ disappear after acid leaching, indicating that SiO_2 is removed. Additionally, the diffraction peaks of perovskite exhibit increased intensities, indicating that perovskite is purified by removing Al_2O_3, SiO_2, and Na_2O. Figure 12 shows the microstructures of different leaching residues. It can be seen that the alkaline-leaching residue is mainly spherical and has good dispersion. The acid-leaching residue is severely agglomerated and the particle size is decreased.

From the above research, we proposed a novel process for the recovery Al_2O_3 and TiO_2 from red mud smelting separation slag, including mineral phase reconstruction-alkaline leaching to extract Al_2O_3 and hydrochloric acid leaching to recover TiO_2. The elements balance in the full flowsheet are presented in Figure 13. The Al_2O_3 is extracted in sodium aluminate solution at an overall Al_2O_3 extraction of 84.91% after alkaline leaching and TiO_2 is recovered in perovskite concentrate assaying 46.53% TiO_2 at an overall TiO_2 recovery of 95.46%.

Table 6. The main chemical composition of various leaching residues (%).

Sample	Fe	Al_2O_3	SiO_2	CaO	MgO	K_2O	Na_2O	TiO_2
Alkaline leaching	4.70	12.71	14.58	16.81	0.72	0.079	14.54	17.97
Acid leaching	6.04	4.80	0.81	37.21	0.80	0.012	1.15	46.53

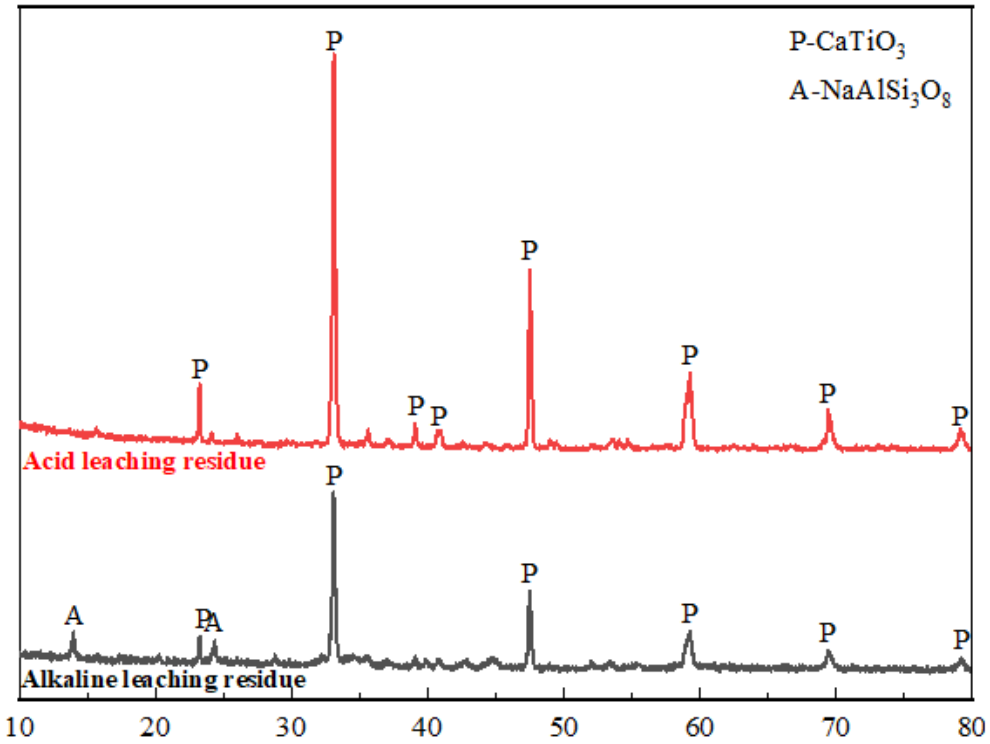


Figure 11. XRD pattern of various leaching residues.

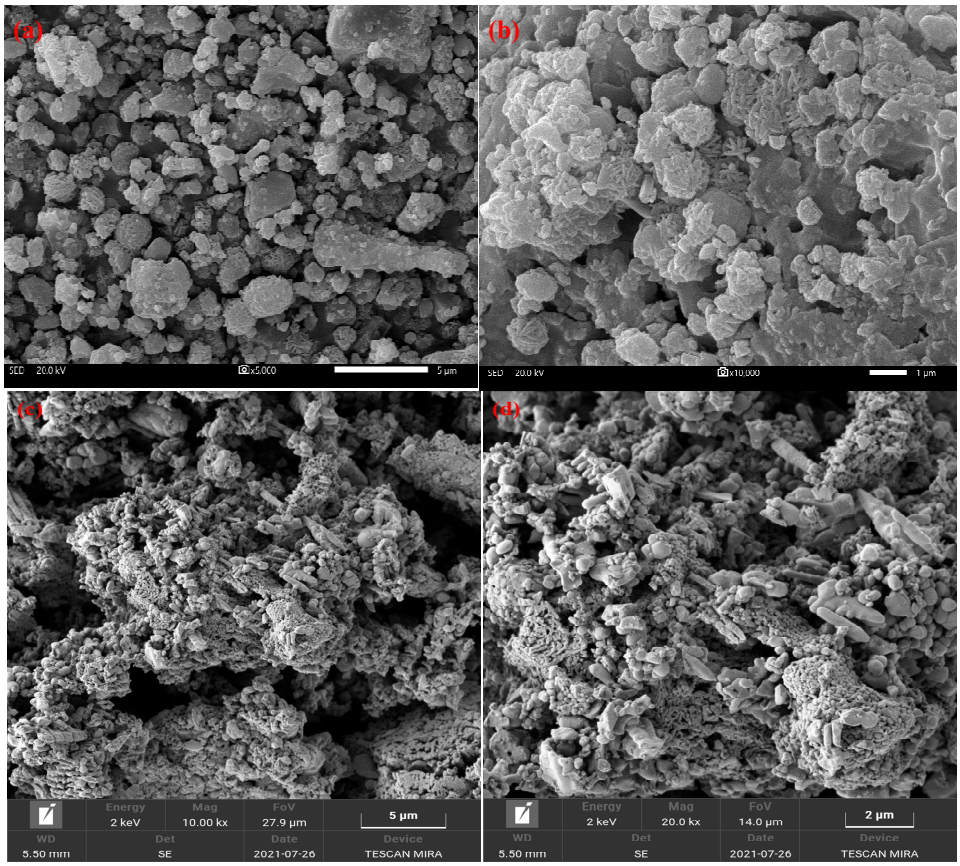


Figure 12. Microstructure of different leaching residues ((**a**,**b**): alkaline leaching slag; (**c**,**d**): acid leaching slag).

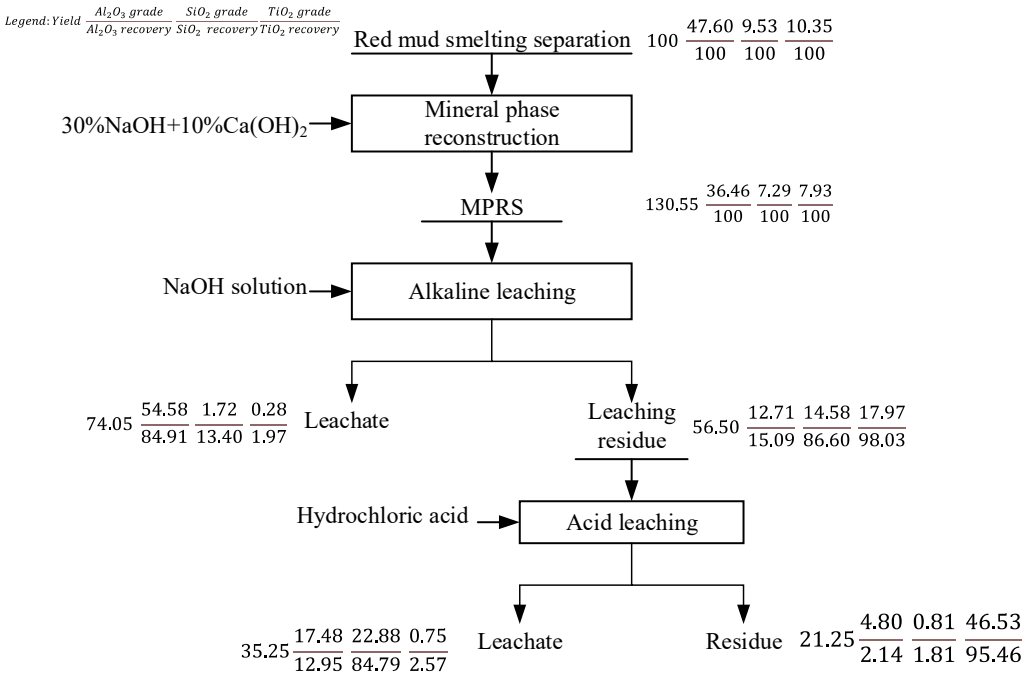


Figure 13. Elements balance in the full sheet.

4. Conclusions

A smelting separation slag obtained from the Bayer red mud by pre-reduction-smelting separation was used as a raw material to extract Al_2O_3. Alumina mainly existed as corundum, a difficult-to-extract phase by simple alkaline leaching. Therefore, a novel process was proposed to selectively extract Al_2O_3 based on mineral phase reconstruction, converting the existing chemical forms of valuable metals for stepwise extraction. The following conclusions can be drawn: in the mineral phase reconstruction process, the NaOH and $Ca(OH)_2$ roasting of Al_2O_3 and $NaAlSiO_4$ was performed.

Under the optimal conditions, i.e., a temperature at 1200 °C, a roasting time of 60 min, and the addition of 30% NaOH + 10% $Ca(OH)_2$, Al-bearing minerals were roasted to $NaAlO_2$, and Si-bearing minerals were transformed to Ca_2SiO_4, respectively. After the mineral phase reconstruction process, Al could be selectively extracted by alkaline leaching under a low temperature with good separation results: the Al_2O_3 recovery rate was 84.91%, and the leaching rate of SiO_2 was 13.40%. The $NaAlO_2$ solution can be used as the source for extracting alumina. Meanwhile, the leaching residue containing high contents of CaO and TiO_2 was further treated to enrich the perovskite phase. By using a 20 wt.% HCl solution, SiO_2 and Al_2O_3 were selectively removed, while 37.21% CaO and 46.53% TiO_2 were enriched in the residue as a raw material for the perovskite phase. The new process can be easily translated to industrial production, where the mineral phase reconstruction process can be achieved by modifying the Na- and Ca-additive roasting procedure in the traditional process.

Author Contributions: Funding acquisition, D.Z. and Z.G.; investigation, S.L. (Siwei Li), T.D. and S.L. (Shenghu Lu); methodology, J.P. and D.Z.; supervision, J.P., D.Z. and Z.G.; writing-original draft, S.L. (Siwei Li); writing-review and editing, S.L. (Shenghu Lu). All authors have read and agreed to the published version of the manuscript.

Funding: This work was financially supported by the Youth natural science foundation China (No.51904347), an Innovation-driven Project of Guangxi Zhuang Autonomous Region (No.AA18242003, No.AA148242003).

Data Availability Statement: The data that generated and/or analysed during the current study are not publicly available due the data is confidential, but are available from the corresponding author on reasonable request.

Acknowledgments: The authors would like to thank Co-Innovation Center for Clean and Efficient Utilization of Strategic Metal Minerals Resources of Hunan Provinces.

Conflicts of Interest: The authors declare no conflict of interest.

References

1. Khairul, M.A.; Zanganeh, J.; Moghtaderi, B. The composition, recycling and utilization of Bayer red mud. *Resour. Conserv. Recycl.* **2019**, *141*, 483–498. [CrossRef]
2. Mukiza, E.; Zhang, L.L.; Liu, X.M.; Zhang, N. Utilization of red mud in road base and subgrade materials: A review. *Resour. Conserv. Recycl.* **2019**, *141*, 187–199. [CrossRef]
3. Ghalehnovi, M.; Roshan, N.; Hakak, E.; Shamsabadi, E.A.; De brito, J. Effect of red mud (bauxite residue) as cement replacement on the properties of self-compacting concrete incorporating various fillers. *J. Clean. Prod.* **2019**, *240*, 118213. [CrossRef]
4. Available online: https://international-aluminium.org/statistics/alumina-production/ (accessed on 12 December 2022).
5. Wang, S.H.; Jin, H.X.; Deng, Y.; Xiao, Y.D. Comprehensive utilization status of red mud in China: A critical review. *J. Clean. Prod.* **2020**, *289*, 125136. [CrossRef]
6. Liu, P.; Shao, G.H.; Huang, R.P. Treatment of Bayer-process red mud through Microbially induced carbonte precipitation. *J. Mater. Civ. Eng.* **2021**, *33*, 04021067. [CrossRef]
7. Nie, Q.K.; Hu, W.; Huang, B.S.; Shu, X.; He, Q. Synergistic utilization of red mud for flue-gas desulfurization and fly ash-based geopolymer preparation. *J. Hazard. Mater.* **2019**, *369*, 503–511. [CrossRef] [PubMed]
8. Huang, Y.F.; Chai, W.C.; Han, G.H.; Wang, W.J.; Yang, S.Z.; Liu, J.T. A perspective of stepwise utilization of Bayer red mud: Step two—Extracting and recovering Ti from Ti-enriched tailing with acid leaching and precipitate flotation. *J. Hazard. Mater.* **2016**, *307*, 318–327.
9. Wang, M.F.; Liu, X.M. Applications of red mud as an environmental remediation material: A review. *J. Hazard. Mater.* **2020**, *408*, 124420. [CrossRef]
10. Liu, S.H.; Guan, X.M.; Zhang, S.S.; Dou, Z.Z.; Feng, C.H.; Zhang, H.B.; Luo, S.Q. Sintered bayer red mud based ceramic bricks: Microstructure evolution and alkalis immobilization mechanism. *Ceram. Int.* **2017**, *43*, 13004–13008. [CrossRef]
11. Ding, W.; Xiao, J.H.; Peng, Y.; Shen, S.Y.; Chen, T. Iron extraction from red mud using roasting with sodium salt. *Miner. Process. Extr. Metall. Rev.* **2019**, *42*, 153–161.
12. Shrey, A.; Veeranjaneyulu, R.; Nikhil, D. Microwave Reduction of Red Mud for Recovery of Iron Values. *J. Sustain. Metall.* **2018**, *4*, 427–436.
13. Valeev, D.; Zinoveev, D.; Kondratiev, A.; Lubyanoi, D.; Pankratov, D. Reductive Smelting of Neutralized Red Mud for Iron Recovery and Produced Pig Iron for Heat-Resistant Castings. *Metals* **2019**, *10*, 32. [CrossRef]
14. Gao, Y.J.; Liang, K.; Gou, Y.; Wei, S.A.; Shen, W.F.; Cheng, F.Q. Aluminum extraction technologies from high aluminum fly ash. *Rev. Chem. Eng.* **2021**, *37*, 885–906. [CrossRef]
15. Kudyba, A.; Akhtar, S.; Johansen, I.; Safarian, J. Aluminum recovery from white aluminum dross by a mechanically activated phase separation and remelting process. *JOM* **2021**, *73*, 2625–2634. [CrossRef]
16. Zinoveev, D.; Pasechnik, L.; Fedotov, M.; Dyubanov, V.; Grudinsky, P.; Alpatov, A. Extraction of valuable elements from red mud with a focus on using liquid media—A review. *Recycling* **2021**, *6*, 38. [CrossRef]
17. Bayca, S.U.; Kisik, H. Optimization of leaching parameters of aluminum hydroxide extraction from bauxite waste using the Taguchi method. *Environ. Prog. Sustain. Energy* **2018**, *37*, 196–202. [CrossRef]
18. Pasechnik, L.A.; Skachkov, V.M.; Bogdanova, E.A.; Chufarov, A.Y.; Kellerman, D.G.; Medyankina, I.S.; Yatsenko, S.P. A promising process for transformation of hematite to magnetite with simultaneous dissolution of alumina from red mud in alkaline mediumAutoclave hydrometallurgical processing of alumina production red mud. *Hydrometallurgy* **2020**, *196*, 105438. [CrossRef]
19. Li, S.W.; Pan, J.; Zhu, D.Q.; Guo, Z.Q.; Shi, Y.; Dong, T.; Lu, S.H.; Tian, H.Y. A new route for separation and recovery of Fe, Al and Ti from red mud. *Resour. Conserv. Recycl.* **2020**, *168*, 105314. [CrossRef]
20. Yang, H.; Shen, S.F.; Liu, H.Y.; Zhen, X.J.; Li, W.G.; Zhao, Q.C.; Wang, J.L.; Luo, Y.F. Study on Mineralogical Characteristics of Secondary Aluminum Ash. *Nonferrous Met. Eng.* **2019**, *9*, 117–124. (In Chinese)
21. Sun, Y.L.; Liang, Z.K.; Qi, G.X.; Xu, H.; Li, L.; Yuan, C.; Wang, Y. Optimization of reaction conditions and mechanism of desilication of high-alumina fly ash. *Res. Environ. Sci.* **2016**, *29*, 753–760. (In Chinese)
22. Guo, W.; Li, D.X.; Yang, N.R. Ions dissolving-out characteristics of calcined coal gangues in alkaline solutions and its structure. *J. Chin. Ceram. Soc.* **2004**, *32*, 1230–1234. (In Chinese)
23. Sitarz, M.; Handke, M.; Mozgawa, W.; Galuskin, E.; Galuskin, I. The non-ring cations influence on silicooxygen ring vibrations. *J. Mol. Struct.* **2000**, *555*, 357–362. [CrossRef]
24. Jin, X.H.; Gao, L.; Guo, J.K. The structural change of diphasic mullite gel studied by XRD and IR spectrum analysis. *J. Eur. Ceram. Soc.* **2002**, *22*, 1307–1311. [CrossRef]

25. Li, C.; Wan, J.H.; Sun, H.H.; Li, L.T. Investigation on the activation of coal gangue by a new compound method. *J. Hazard. Mater.* **2010**, *179*, 515–520. [CrossRef] [PubMed]
26. Song, X.Y.; Gong, C.C.; Li, D.X. Study on structural characteristic and mechanical property of coal gangue in the activation process. *J. Chin. Ceram. Soc.* **2004**, *32*, 358–363.
27. Guo, W.; Li, D.X.; Chen, J.H.; Yang, N.R. Structure and pozzolanic activity of calcined coal gangue during the process of mechanical activation. *J. Wuhan Univ. Technol.* **2009**, *24*, 326–329. [CrossRef]
28. Brachhold, N.; Koning, A.S.; Brendler, E.; Aneziris, C. Investigation of the synthesis and the alkali corrosion of potassium aluminosilicates by XRD and NMR. *Ceram. Int.* **2021**, *47*, 33596–33605. [CrossRef]
29. Gupta, R.; Tomar, A.S.; Mishra, D.; Sanghi, S.K. Multinuclear MAS NMR characterization of fly-ash-based advanced sodium aluminosilicate geopolymer: Exploring solid-state reactions. *Chemistryselect* **2020**, *5*, 4920–4927. [CrossRef]
30. Chun, T.J.; Zhu, D.Q.; Pan, J.; He, Z. Recovery of Alumina from Magnetic Separation Tailings of Red Mud by Na_2CO_3 Solution Leaching. *Metall. Mater. Trans. B.* **2014**, *45*, 827–832. [CrossRef]

Disclaimer/Publisher's Note: The statements, opinions and data contained in all publications are solely those of the individual author(s) and contributor(s) and not of MDPI and/or the editor(s). MDPI and/or the editor(s) disclaim responsibility for any injury to people or property resulting from any ideas, methods, instructions or products referred to in the content.